ACS APPLIED ENERGY MATERIALS

www.acsaem.org Article

One-Step Facile Synthesis of High-Activity Nitrogen-Doped PtNiN Oxygen Reduction Catalyst

Liang Song, Yun Cai, Yang Liu, Xueru Zhao, Kurian A. Kuttiyiel, Nebojsa Marinkovic, Anatoly I. Frenkel, Anusorn Kongkanand, YongMan Choi, Radoslav R. Adzic, and Kotaro Sasaki*

Cite This: *ACS Appl. Energy Mater.* 2022, 5, 5245−5255 Read Online

ACCESS | Metrics & More | Article Recommendations | Supporting Information

ABSTRACT: PtM alloy electrocatalysts (M = Fe, Co, Ni) have been the subject of many investigations aimed at increasing their attractive properties, in particular their oxygen reduction reaction (ORR) activity, while reducing total platinum-group-metal content and improving durability. Despite some success, these catalysts still have relatively high Pt content and lack the necessary durability, as M metals leach out from the alloys during potential cycling. Previously, we synthesized nitrogen (N)-doped PtMN/C catalysts consisting of thin Pt shells on M nitride cores by a two-step method, which showed higher ORR activity and stability than their PtM counterparts. In the present study, we developed a facile one-step synthesis method, which comprises a single thermal annealing process of the N-doped PtNiN/C alloy. The ORR performance of the one-step-synthesized PtNiN/C catalyst is much higher than that of the two-step-synthesized PtNiN/C, as revealed by rotating disk electrode measurements. Membrane electrode assembly fuel cell testing demonstrated superb durability and high activity. Formation of Pt monolayer shells on the nitrided $(Pt_xNi_{1-x})_4N$ cores was confirmed by *in situ* X-ray absorption spectroscopy. The origins of the enhanced activity and stability of the one-step-synthesized PtNiN/C catalyst are elucidated based on density functional theory calculations together with the experimental results.

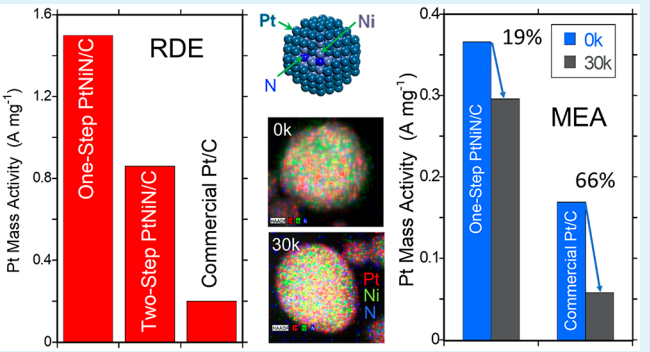

KEYWORDS: *one-step synthesis, fuel cells, oxygen reduction, platinum−nickel nanoparticles, nitrogen doping, rotating disk electrode, membrane electrode assembly*

INTRODUCTION

In spite of significant advances in recent years, the present cathode catalysts for proton exchange membrane fuel cells (PEMFCs) have two drawbacks. One is the insufficient efficiency of energy conversion, and the other is the high platinum (Pt) content in the electrocatalyst.[1−3] The sluggish kinetics of the oxygen reduction reaction (ORR) is considered the principal cause of both problems. Therefore, many reaction sites (*i.e.*, high cathode Pt loadings) are required to enable practical power densities for commercial PEMFC applications. Another main problem is the dissolution of Pt nanoparticles during potential cycling, which occurs in automotive fuel cell applications.[4] Reducing the Pt content and lowering Pt dissolution are essential to obtain cost-effective, durable fuel cell systems. Recent great advance in electrocatalysis involves developing a Pt monolayer (ML) electrocatalyst by reducing the overall amount of Pt by a Pt ML shell on an appropriate nanoparticle core.[5−8] Particularly, a Pt ML over a Pd core (Pt_{ML}/Pd/C) has an extremely low Pt loading with high activity and durability. This research has stimulated broader studies of core−shell catalysts. However, the recent rise in Pd cost is a drawback of the Pt_{ML}/Pd/C catalysts,[9] and therefore, developing stable platinum-group-metal (PGM)-free cores for thin Pt shells is desirable.

Pt-alloy-based electrocatalysts have been investigated to exploit high ORR activity while reducing total PGM content and improving durability.[10−13] While platinum−metal (Pt−M, where M = Fe, Co, Ni) structures show high initial activity, these catalysts still require a high Pt content and lack durability, as M metals leach out from the alloy during potential cycling. We previously reported the synthesis and ORR performance of core−shell nanoparticles comprising a Pt shell on an M nitride core.[14,15] The synthesis consisted of two processes, *i.e.*, a chemical reduction process in an aqueous solution and subsequent thermal annealing in argon and then ammonia (NH_3) gases. Nitriding through nitrogen (N) reacting with selected elements can form M nitrides (such as

Received: February 28, 2022
Accepted: March 30, 2022
Published: April 14, 2022

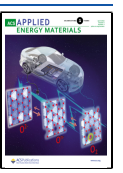

https://doi.org/10.1021/acsaem.2c00631
ACS Appl. Energy Mater. 2022, 5, 5245−5255

Ni_4N) with a variety of intriguing properties, including high electrochemical stability. The ORR activity and durability of the PtMN catalysts are higher than those of Pt−M-alloy-structured catalysts. Among them, the PtNiN/C catalyst showed the highest ORR performance.[15]

One-step synthesis could potentially improve the quantity and reduce production time and cost compared with multistep synthesis routes.[16] Recently, we developed a more facile synthesis method comprising a single thermal annealing process to synthesize the N-doped PtNiN/C catalyst. By avoiding the chemical reduction procedure in aqueous media, the risk of oxidizing the Ni cores is eliminated. The resulting catalyst showed higher ORR activity and durability in rotating disk electrode (RDE) measurements than those previously reported.[14,15] In this study, membrane electrode assembly (MEA) fuel cell tests were performed, demonstrating the promise of this highly durable low-PGM ORR electrocatalyst for PEMFCs. *In situ* X-ray absorption spectroscopy (XAS) revealed that the atomic structure of the PtNiN/C catalyst consists of PtNiN nitride cores encapsulated by Pt ML shells. These experimental results coupled with density functional theory (DFT) calculations revealed the origins of the high ORR performance of the PtNiN/C catalyst synthesized by the one-step method. The establishment of scale-up synthesis methodology up to a few grams is an essential step from an RDE test to a MEA fuel cell test in real conditions, and the new one-step method could promote the high-efficient N-doped PtNiN catalyst toward commercial viability.

EXPERIMENTAL SECTION

Materials and Chemicals. The materials used in this study include Vulcan XC72R carbon black from Cabot Corp., platinum(II) 2,4-pentanedionate ($Pt(acac)_2$), 2,4-pentanedionate nickel(II) ($Ni(acac)_2$), and acetone (C_3H_6O, ≥99.5%) from Sigma-Aldrich, commercial Pt/C (46.4 wt % Pt) from Tanaka Kikinzoku Kogyo (TKK), and Ar (99.999%), O_2 (99.6%), CO (99.99%), and NH_3 (99.9995%) gases from Praxair Inc. All solutions in this study were prepared using Millipore ultrapure water (18.2 MΩ·cm). The detailed procedure of the one-step synthesis is described in the Results and Discussion section. Energy-dispersive X-ray (EDX) analysis of the one-step-synthesized catalyst showed 20.3 wt % Pt and 3.9 wt % Ni (balance C), reflecting a Pt:Ni mole ratio of 60:40. Thermogravimetric analysis (TGA) of the one-step catalyst showed a total metal loading of 24.3 wt %, which is in good agreement with the EDX result (24.2 wt % for Pt and Ni). Carbon−hydrogen−nitrogen (CHN) analysis revealed 0.17 wt % nitrogen (N) in the catalyst, reflecting a Ni/N atomic ratio of 5.5.

RDE Measurements. PtNiN/C catalyst (5 mg) was dispersed in a 5 mL solution of 3:1 water:isopropanol with 5 μL of Nafion (perfluorinated resin, 5 wt % in H_2O, Sigma-Aldrich) to prepare the catalyst ink. The Pt loading on the RDE was 20 μg cm^{-2}. RDE measurements were made in a conventional three-electrode electrochemical cell at room temperature, where an RDE with the catalyst was used as a working electrode, with a Pt counter electrode and a Ag/AgCl in 3 M KCl reference electrode connected via a salt bridge. Cyclic voltammetry (CV) was conducted in an Ar-purged 0.1 M $HClO_4$ electrolyte at a scan rate of 20 mV s^{-1}, while ORR polarization measurements were made in an O_2-purged 0.1 M $HClO_4$ solution at 10 mV s^{-1} with a rotation rate of 1600 rpm. Accelerated durability tests (ADTs) were conducted in an aerated 0.1 M $HClO_4$ solution under potential cycling between 0.6 and 1 V with a scan rate of 50 mV s^{-1} for up to 30 000 cycles. All the potentials are reported with respect to a reversible hydrogen electrode (RHE).

MEA Fuel Cell Measurements. MEAs with an active area of 50 cm^2 were fabricated by hot pressing electrode decals at 310 °C and 5000 lb. to the membrane for 5 min. The membrane used for this study is an 18 μm thick perfluorosulfonic acid (PFSA) membrane with an internal reinforcement layer. The electrodes were fabricated with an ionomer to carbon (I/C) (w/w) ratio of 0.6 on the anode and 0.9 on the cathode. The anode (20 wt % Pt/graphitized carbon) and cathode Pt loadings were 0.05 and 0.1 mg cm^{-2}, respectively. A commercially available ionomer solution (Nafion D2020, EW1000 g eq^{-1}, DuPont) was used for all cathodes. MEAs were assembled into the cell hardware for performance and durability tests with 235 μm thick carbon paper gas diffusion layers (GDLs) on both the anode and cathode. The detailed procedures for the electrode and MEA fabrication are reported elsewhere.[17] The test conditions for fuel cell performance were 80 °C, 100% relative humidity (RH), and 150 $kPa_{abs,outlet}$ in either H_2/O_2 or H_2/air. The ORR mass activity was calculated at 0.9 V (high-frequency-resistance-corrected) from the H_2/O_2 polarization curve.[17] The cathode Pt electrochemical surface area (ECSA) was determined by integrating hydrogen adsorption peaks (assuming 210 μC cm^{-2} Pt) from CV measured while the cell was operated at 30 °C, 101 kPa_{abs}, and 100% RH in H_2/N_2. The fuel cell durability tests were made by cycling the cells in H_2/N_2 at 80 °C, 100% RH, and 101 kPa_{abs} for 30 000 cycles between the upper voltage of 0.95 V and lower voltage of 0.60 V for 3 s at each potential. BOL (beginning of life) and EOL (end of life) performance tests were conducted before and after these voltage-cycling tests.

Materials Characterization. Transmission electron microscopy (TEM), high-angle annular dark-field scanning transmission electron microscopy (HAADF-STEM), and energy-dispersive spectroscopy (EDS) elemental mapping images were obtained using an FEI Talos 200× TEM at an accelerating voltage of 200 kV at the Center for Functional Nanomaterials (CFN), Brookhaven National Laboratory (BNL). X-ray powder diffraction (XRD) patterns were collected on a Rigaku Miniflex II with Cu Kα radiation at the CFN/BNL. *In situ* XAS analysis using an electrochemical cell was carried out at the ISS (8-ID) and QAS (7-BM) beamlines of the National Synchrotron Light Source II (NSLS II) at BNL. The PtNiN/C sample (working electrode), a proton exchange membrane (Nafion 117, DuPont Chemical Co., DE), and a Pt thin foil (counter electrode) were sandwiched and clamped tightly between two acrylic plastic bodies. Each plastic body had an X-ray transparent window. The electrolyte was 1 M $HClO_4$, and a Ag/AgCl leak-free electrode was used as a reference electrode. Details of the electrochemical cell and experimental procedures are described elsewhere.[18] The XAS data were analyzed by Athena and Artemis software.[19]

Computational Methods. Spin-polarized density functional theory (DFT) calculations were carried out using the Vienna ab initio simulation package (VASP)[20] with the generalized gradient approximation (GGA) using the revised Perdew-Burke-Ernzerhof (RPBE) functional[21] and the projector-augmented wave method (PAW) similar to our previous studies.[14,15] The dissolution potentials of the Pt shell in acidic media were calculated for examination of the stability.[5,22] More details are given in the Supporting Information.

RESULTS AND DISCUSSION

One-Step Synthesis. Carbon-supported PtNiN electrocatalysts were prepared by the following one-step method (Figure 1a): Metal precursors ($Pt(acac)_2$) and ($Ni(acac)_2$) were mixed with Vulcan XC72R carbon in acetone. The mole ratio of Pt:Ni in the precursors was 1:1. For example, 316 mg of $Pt(acac)_2$, 209 mg of $Ni(acac)_2$, and 475 mg of carbon (total 1 g) were mixed in ∼300 mL of acetone. The mixed solution was first stirred by using a magnetic stirrer for 1 h, followed by ultrasonication for 30 min. The mixture was dried using a rotary evaporator in a heating bath at 50 °C. The dried sample was annealed in a furnace at 510 °C for 2 h under a 200 sccm NH_3 gas flow. Finally, the catalyst sample was cooled to room temperature under the same NH_3 flow in the furnace and then purged sufficiently with Ar before being collected for further characterization. The EDX, TGS, and CHN analyses of the product showed 20.3 wt % Pt, 3.9 wt % Ni, and 0.17 wt % N

https://doi.org/10.1021/acsaem.2c00631
ACS Appl. Energy Mater. 2022, 5, 5245−5255

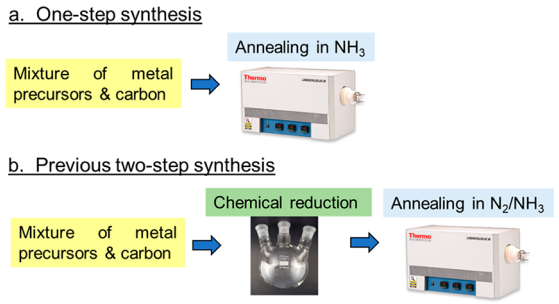

Figure 1. Comparison of (a) the present one-step synthesis and (b) the previous two-step synthesis.[14,15]

(balance C), reflecting a Pt:Ni mole ratio of 6:4 and a Ni:N mole ratio of 5.5:1 (*i.e.*, Ni/N = 5.5). The one-step synthesis is much simpler and shorter than the previous two-step synthesis consisting of separate chemical reduction by sodium borohydride ($NaBH_4$) in an aqueous solution and thermal annealing steps (in N_2 at 250 °C for 1 h and NH_3 at 510 °C for 2 h) (Figure 1b),[15] making it more applicable for synthesis of more than 1 g. It is considered that the longer annealing in addition to the chemical reduction process in the two-step synthesis may have generated the Ni-rich (Ni_4N) core.

Morphology of PtNiN/C. As shown in TEM images in Figure 2a,b, the PtNiN particles synthesized by the one-step method are monodispersed on the Vulcan carbon supports. The XRD pattern of the PtNiN/C is shown in Figure 2c. The average particle diameter is calculated to be about 3.5 nm using the Scherrer equation, and the lattice constant of the face-centered-cubic (fcc) structure is determined to be 3.736 Å (0.3736 nm). Figure 2d–f shows EDS mapping images of Pt, Ni, and N of a PtNiN particle, respectively, and Figure 2g shows a corresponding HAADF-STEM image with EDS mapping of PtNiN elements; they clearly illustrate well-mixed Pt and Ni atoms with N atoms in the particle, although a partition between a shell and a core is unclear. As discussed later, *in situ* XAS analysis revealed the formation of a core–shell structure comprising Pt ML shells on $(PtNi)_4N$-type cores.

ORR Performance of PtNiN/C by RDE Testing. The ORR electrocatalytic activity and durability of the PtNiN/C were studied by measuring ORR polarization curves in O_2-purged 0.1 M $HClO_4$ at a sweep rate of 10 mV s^{-1} using RDE at a rotation rate of 1600 rpm (Figure 3a). To determine the mass activity (MA), the kinetic current was normalized to the Pt loading. The specific activity (SA) was calculated by normalizing the current to the ECSA by measuring the charge derived from the H_{upd} adsorption region after double-layer correction (Figure 3b).[23] The PtNiN/C showed Pt MA and SA of 1.50 A mg^{-1} and 1.69 mA cm^{-2} at 0.9 V; they are higher than those of the PtNiN/C catalyst synthesized by our previous two-step method (0.86 A mg^{-1} and 1.65 mA cm^{-2}) and are also approximately 7.5 and 7 times higher than those of a commercial Pt/C catalyst (0.20 A mg^{-1} and 0.24 mA cm^{-2}, respectively[14,15]). The half-wave potential ($E_{1/2}$) and the ECSA of the PtNiN catalyst are 932 mV and 89 m^2 g^{-1}, which are also greater than those of the two-step-synthesized PtNiN/C (905 mV and 52 m^2 g^{-1}) and the commercial Pt/C (850 mV and 83 m^2 g^{-1}).[14,15] ADTs were carried out by applying potential sweeps between 0.6 and 1.0 V at 50 mV s^{-1} in aerated 0.1 M $HClO_4$ as shown in Figure 3a,b. After 30 000 cycles, the ORR and CV measurements exhibited small losses in MA (−30%), SA (−20%), $E_{1/2}$ (−13 mV), and ECSA (−13%), indicating that the PtNiN/C catalyst prepared by the one-step method has very good ORR durability. The results are listed in Table 1. The morphology of the PtNiN/C at EOL is shown in Figure S1. The TEM images (Figure S1a,b) show the appearance of some large particles as a consequence of particle coalescence and/or electrochemical Ostwald ripening.[4] The

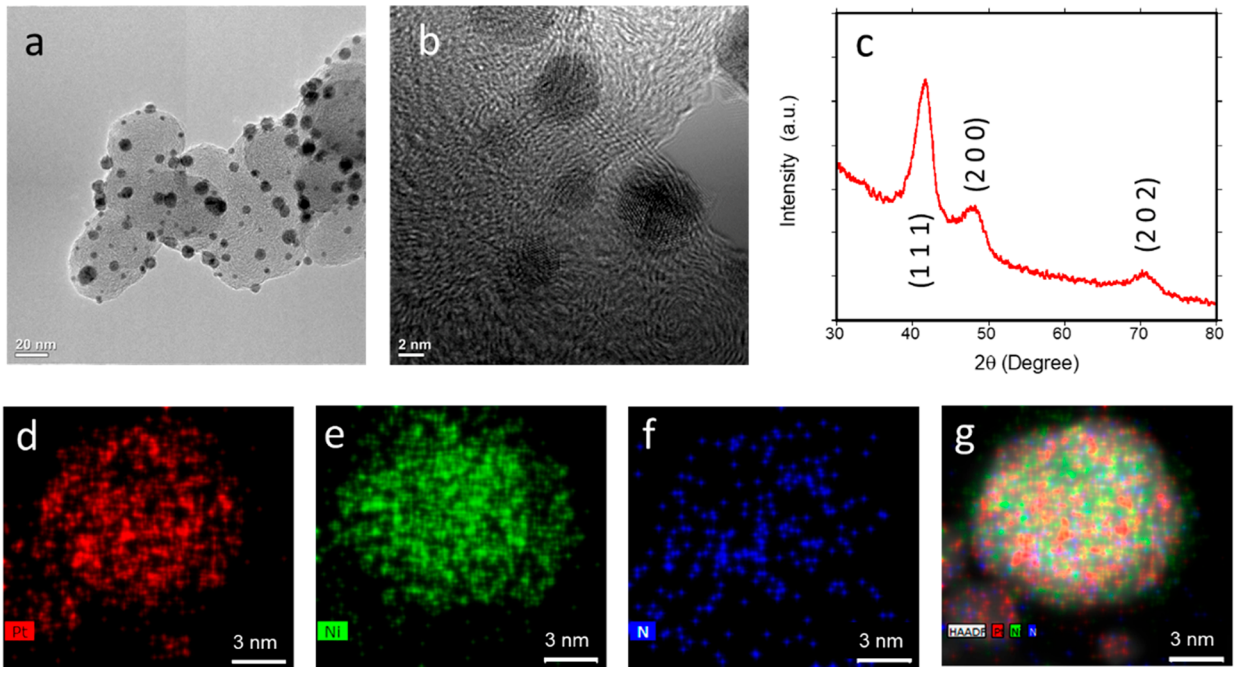

Figure 2. (a,b) TEM images of PtNiN nanoparticles on Vulcan XC72R carbon. (c) XRD pattern of the PtNiN/C catalyst (using Cu Kα). (d–f) EDS mapping images of Pt, Ni, and N of a PtNiN particle, respectively, and (g) a corresponding HAADF-STEM image with EDS mapping of PtNiN elements.

https://doi.org/10.1021/acsaem.2c00631
ACS Appl. Energy Mater. 2022, 5, 5245−5255

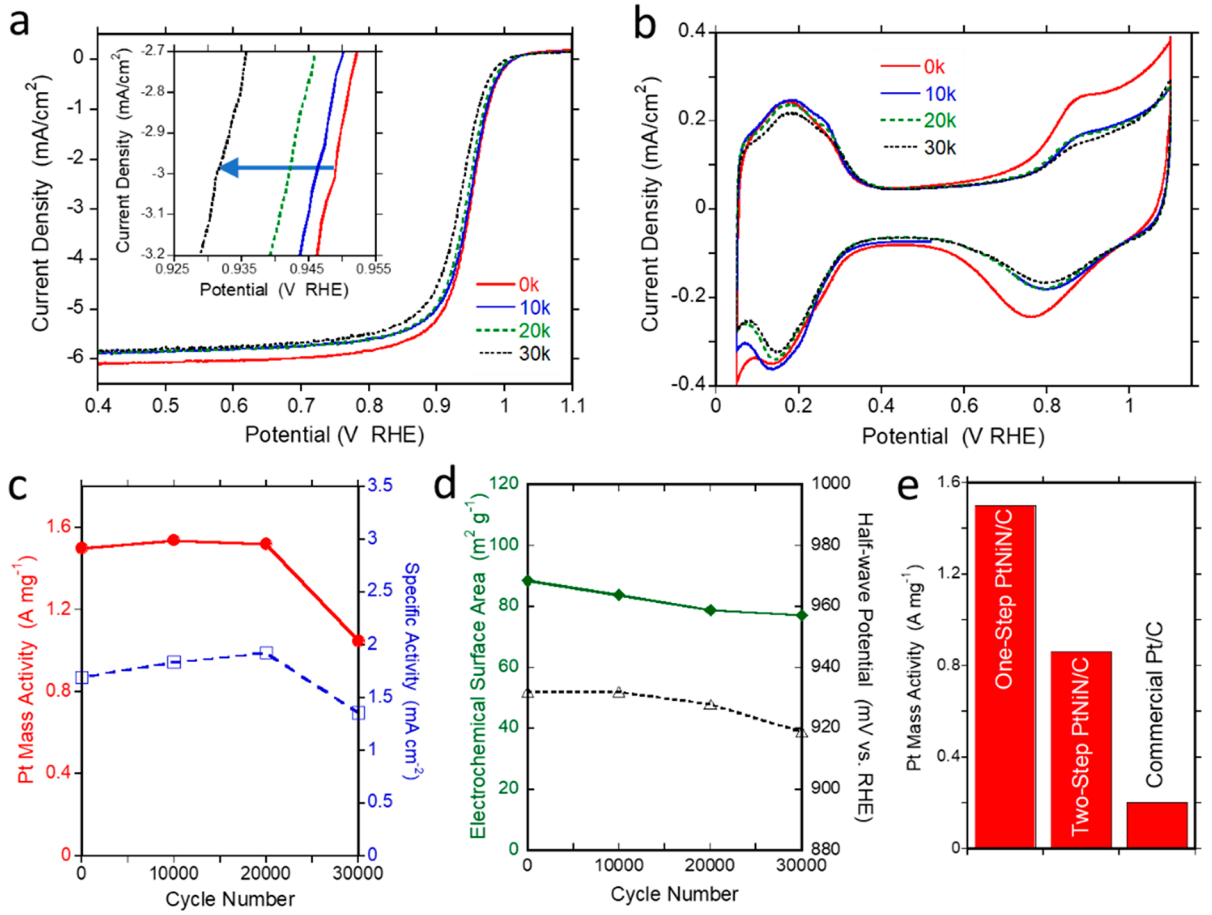

Figure 3. RDE results of PtNiN/C synthesized by the one-step method, including (a) ORR polarization curves measured in O_2-purged 0.1 M $HClO_4$ at a scanning rate of 10 mV s^{-1} at a rotation rate of 1600 rpm and (b) CV curves obtained in Ar-purged 0.1 M $HClO_4$ at a scanning rate of 20 mV s^{-1} before and after 10 000, 20 000, and 30 000 cycles. Changes in (c) MA and SA and (d) ECSA and $E_{1/2}$ plotted versus the number of potential cycles. (e) Pt MA of one-step-synthesized PtNiN/C, two-step-synthesized PtNiN/C, and commercial Pt/C.

Table 1. List of MA, SA, $E_{1/2}$, and ECSA of One-Step-Synthesized PtNiN/C in RDE Testing[a]

cycle number	MA (A mg^{-1})	SA (mA cm^{-2})	$E_{1/2}$ (mV vs RHE)	ECSA (m^2 g^{-1})
0	1.50 (0.86)	1.69 (1.60)	932 (905)	89 (52)
10 000	1.54	1.83	932	84
20 000	1.52	1.93	928	79
30 000	1.05	1.36	919	77
loss ($C_{30k} - C_0$)/C_0 × 100	−30%	−20%	−13 mV ($E_{1/2\_30k} - E_{1/2\_0}$)	−13%

[a]Numbers in parentheses are those of two-step-synthesized PtNiN/C.[14,15]

EDS mapping images (Figure S1c–f) show the thickening of Pt shells to a couple of atomic layers due to leaching of Ni atoms from the cores.[4]

The ORR performance of the PtNiN/C is also higher than those of an alloy-structured PtNi/C catalyst (without N) (MA = 0.46 A mg^{-1} and MA loss after 30 000 cycles = −65.2%).[24] Alloying Pt with Ni induces high lattice contraction (lattice constant of 3.715 Å (0.3715 nm)) because of the smaller diameter of the Ni atoms.[24] As discussed in the section of XAS analysis below, doped-N atoms occupy the center of the fcc structure, which alleviates the degree of contraction (3.736 Å (0.3736 nm)). This results in the optimal adsorption strength for intermediates during the ORR, which gives rise to the enhanced ORR activity. Changes in lattice parameter by alloying with Ni and N-doping are schematically shown in Figure S2. One possible reason for the enhanced durability of the PtNiN/C is the formation of chemically stable Ni−N bonds.[24] A detailed rationale for the difference in ORR performance between the one-step and two-step methods will be discussed based on the DFT studies below.

MEA Performance of PtNiN/C. MEA fuel cell tests (50 cm^2) of the PtNiN/C catalyst were performed at General Motors (GM). Figure 4a shows H_2/O_2 polarization curves after 0, 10 000, and 30 000 potential cycles of the PtNiN/C (red curves) at a back pressure of 150 kPa at 80 °C. Also shown are results from GM's reference PtCo/C (blue curves) and Pt/C (green curves) catalysts, which were measured under the same conditions. These catalysts also employ Vulcan carbon as their supports. The cathode Pt loadings were 0.105, 0.110, and 0.120 mg cm^{-2} for PtNiN/C, PtCo/C, and Pt/C, respectively. The MA of the PtNiN/C catalyst at BOL was 0.366 A mg^{-1}, which is lower than that of RDE testing (1.50 A mg^{-1}) and the U.S. Department of Energy (DOE) 2020 target (0.44 A mg^{-1}). However, it is higher than those of the reference PtCo/C (0.275 A mg^{-1}) and Pt/C (0.169 A mg^{-1}) catalysts. As shown in Figure 4c, the stability of PtNiN/C in MEA testing was relatively high; the MA at EOL (after 30 000 cycles) was 0.296 A mg^{-1}, which was only a −19% loss and

https://doi.org/10.1021/acsaem.2c00631
ACS Appl. Energy Mater. 2022, 5, 5245−5255

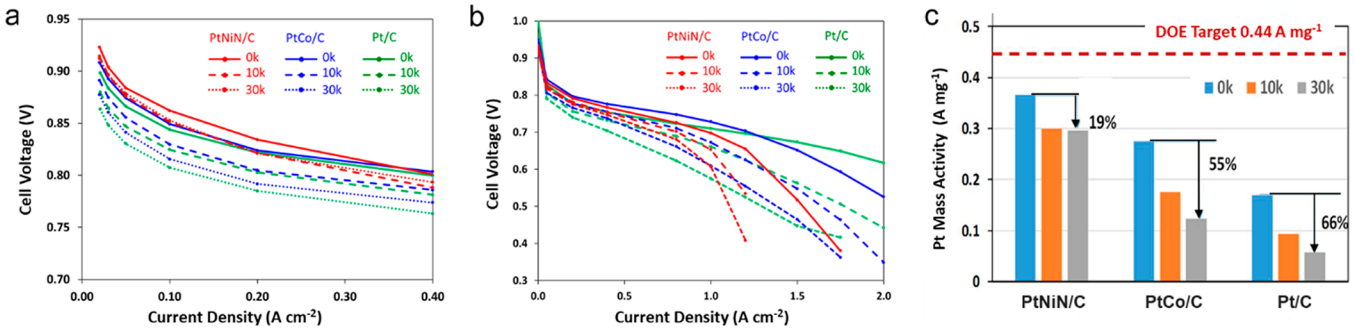

Figure 4. (a) H_2/O_2 and (b) H_2/air polarization curves on MEAs (50 cm^2) assembled with PtNiN/C, PtCo/C, and Pt/C after 0, 10 000, and 30 000 potential cycles, at a back pressure of 150 kPa at 100% RH and 80 °C. Pt loadings at cathodes were 0.105, 0.110, and 0.120 mg cm^{-2} for PtNiN/C, PtCo/C, and Pt/C, respectively. (c) Pt MAs measured at 0.9 V of PtNiN/C, PtCo/C, and Pt/C after 0, 10 000, and 30 000 potential cycles.

exceeded the DOE 2020 target (<40%). The stability of PtNiN/C is superb in comparison with those of PtCo/C and Pt/C, which exhibited losses of 55% (0.124 A mg^{-1}) and 66% (0.058 A mg^{-1}) at EOL, respectively. Although the ECSA of PtNiN/C at BOL (27 m^2 g^{-1}) in MEA testing is much lower than that of RDE testing (89 m^2 g^{-1}), the loss with potential cycling is very small; it is −29% at EOL and is much lower compared to those of PtCo/C (38%) and Pt/C (76%) at EOL (Figure S3). The MEA results are summarized in Table 2.

Table 2. Pt MAs (A mg^{-1}) in MEA Testing of PtNiN/C, PtCo/C, and Pt/C after 0, 10 000, and 30 000 Potential Cycles

cycle number	PtNiN/C	PtCo/C	Pt/C
0	0.366	0.275	0.169
10 000	0.30	0.176	0.093
30 000	0.296	0.124	0.058
loss $(C_{30k} - C_0)/C_0 \times 100$	−19%	−55%	−66%

(Table S1 lists MEA performance at BOL and EOL of different cathode catalysts with different Pt loadings reported in published papers for comparison.) The lower initial ECSA of the PtNiN/C catalyst in the MEA compared to that of the RDE may be due to the challenges of scaling up the synthesis when preparing the required 3 g of materials for MEA testing. A larger furnace with more precise temperature control may address this issue. On the other hand, the fuel cell performance of PtNiN/C under H_2/air, particularly at high current density, was lower than what one would expect from its relatively good MA and ECSA (Figure 4b). As many factors such as catalyst−support pore morphology and ionomer interactions can contribute to high-current-density performance losses besides the activity of the catalyst itself,[25] it is common for any new catalyst to require considerable optimization of the catalyst layer structure, electrode ink preparation, and coating process. This work will be done as a larger amount of catalyst materials become available. In this initial evaluation, the voltage loss at a low current density of 0.05 A cm^{-2} after voltage cycling was much lower than those of PtCo/C and Pt/C (16 vs 37 and 37 mV, respectively), consistent with the MA and ECSA results (Figure S4a). However, its voltage loss at a high-current density region of 1.20 A cm^{-2} was greater (Figure S4b).

***In Situ* XAS of PtNiN/C.** The *in situ* X-ray absorption near edge structure (XANES) spectra for the Ni K-edge of the PtNiN/C catalyst in a 1 M $HClO_4$ solution at different potentials are presented in Figure 5a. The Ni K-edge XANES spectrum of PtNiN/C is different from that of reference Ni, suggesting that the electronic state and atomic structure of Ni in the PtNiN/C are altered by N-doping and alloying with Pt. The extended X-ray absorption fine structure (EXAFS) spectrum in *k*-space (Figure 5b) also demonstrates that the Ni atomic structure in PtNiN/C is different from that of a Ni foil. Furthermore, no clear changes in Ni K-edge XANES of PtNiN/C are observed in a potential range of 0.42−0.92 V in Figure 5a,b, indicating that Ni is protected by the Pt shell from being dissolved/oxidized during the ORR, and the core−shell structure of PtNiN/C nanoparticles remain intact because no apparent change in atomic structure with increasing potentials is observed.

The *in situ* XANES spectra of the Pt L_3-edge of the PtNiN/C at increasing potentials are presented in Figure 5c. The intensity of white lines (the first peaks at Pt L_3 absorption edge) generally increases with rising potentials through depleting the d-band due to the formation of Pt oxide.[18,26,27] The white line intensity of the Pt L_3-edge of PtNiN/C increases with applied potentials, indicating that the catalyst is oxidized with increasing potentials. However, the oxidation is confined only to the Pt shell surface, and the core remains almost intact, since no discernible changes of the Ni K-edge are observed (Figure 5a). This is also a distinct evidence that the PtNiN/C catalyst has the core−shell structure with the Pt shells and Ni-rich cores. The phase in oscillation of the PtNiN/C in Figure 5d is prominently deviated from that of Pt foil in a *k*-range over 8 $Å^{-1}$, representing that the atomic structure of the Pt in PtNiN/C is also very different from a Pt bulk.

The results of the concomitant fitting for the Ni K-edge and Pt L_3-edge data at 0.42 V are shown in Figure 6a,b, respectively. There is a very good agreement between the data and fits. Contributions of Ni−Ni, Ni−Pt, and Ni−N for the Ni fitting are shown in Figure 6a, while contributions of Pt−Pt and Pt−Ni for the Pt fitting are shown in Figure 6b. The best fitting results for coordination numbers (CN), bond lengths (*d*), and bond length disorder parameters (σ^2) for the PtNiN/C catalyst are summarized in Table 3.

The CN of Pt−Pt pairs for PtNiN/C is 6.4 ± 0.6 (Table 3). Previously, we analyzed an atomic structure of a Pt_{ML}/Pd/C catalyst having Pt ML shells on Pd nanoparticles by fitting EXAFS data and determined that the CN of Pt−Pt was 5.8 ± 0.8 (the average particle size is 4.2 nm),[7] which is slightly lower than the number obtained from the present study.

https://doi.org/10.1021/acsaem.2c00631
ACS Appl. Energy Mater. 2022, 5, 5245−5255

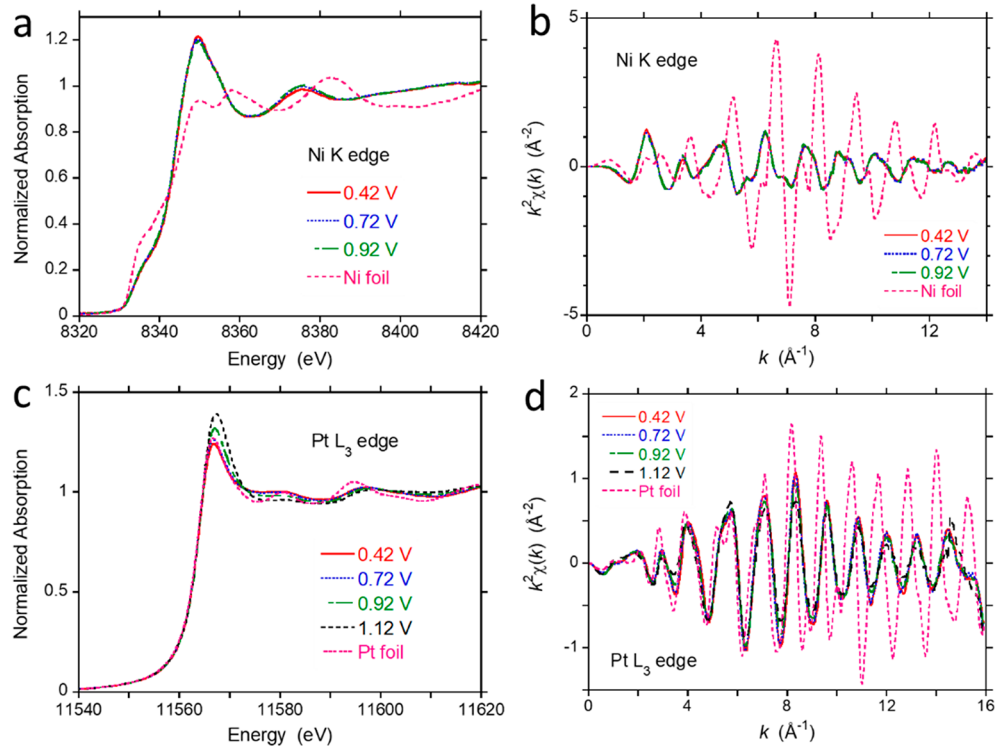

Figure 5. *In situ* Ni K-edge (a) XANES and (b) *k*-space (k^2-weighted) EXAFS spectra of PtNiN/C at different potentials with those of a reference Ni foil. *In situ* Pt L_3-edge (c) XANES and (d) *k*-space (k^2-weighted) EXAFS spectra of PtNiN/C at different potentials with those of a reference Pt foil. The *in situ* XAS data were acquired in 1 M $HClO_4$ using an electrochemical cell.[18]

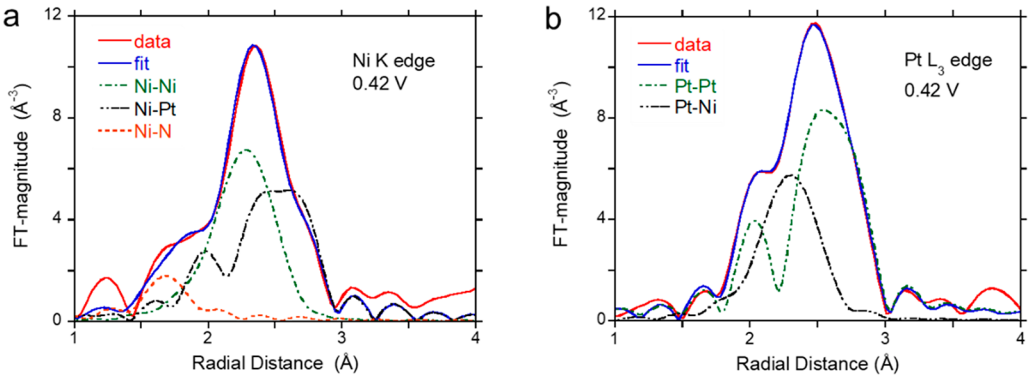

Figure 6. (a) *In situ* Ni K-edge FT-EXAFS with a first-shell fit, together with Ni−Ni, Ni−Pt, and Ni−N contributions at 0.42 V in 1 M $HClO_4$. (b) *In situ* Pt L_3-edge FT-EXAFS with a first-shell fit, together with Pt−Pt and Pt−Ni contributions at 0.42 V in 1 M $HClO_4$.

Table 3. Coordination Numbers (CN), Bond Lengths (*d*), and Bond Length Disorder Parameters (σ^2) for Different First Nearest Neighboring Pairs in PtNiN/C at 0.42 V Determined by the EXAFS Fitting Shown in Figure 6a,b

	CN	*d* (Å)	σ^2 (Å^2)
Pt−Pt	6.4 ± 0.6	2.696 ± 0.003	0.0057 ± 0.0004
Pt−Ni	3.9 ± 0.4	2.632 ± 0.005	0.0086 ± 0.0008
Ni−Ni	3.5 ± 0.9	2.620 ± 0.009	0.0097 ± 0.0024
Ni−Pt	5.8 ± 0.6	2.632 ± 0.005	0.0086 ± 0.0008
Ni−N	3.0 ± 0.8	2.057 ± 0.010	0.0107 ± 0.0055

Proposed Core−Shell Atomic Model of PtNiN/C. Our proposed core−shell atomic model begins with the assumption that the PtNiN catalyst comprises a two-ML Pt shell on a core (Pt 2ML-shell model, Figure 7a). The ratio of surface atoms ($N_{surface}$) to total atoms (N_{total}), as shown in Figure 8b, for a 3.5 nm diameter particle (*i.e.*, the first ML) is 0.35, and that for a 2.98 nm particle (*i.e.*, the second ML; 3.5 − 0.262 × 2) is 0.40. Therefore, the percentage of the combined two ML atoms to total atoms is 61% (= 35 + 0.40 × 65). Since the Pt:Ni mole ratio of the catalyst is 0.6:0.4 (x_{Pt} = 0.60 and x_{Ni} = 0.40), the two ML shell comprises 100% of the total Pt (x^s_{Pt} = 0.60) and 2.5% of the total Ni atoms (x^s_{Ni} = 0.01), and the core consists of the remaining 97.5% Ni atoms (x^c_{Ni} = 0.39) and no Pt (x^c_{Pt} = 0). However, this Pt 2ML-shell model cannot be used to depict the structure of PtNiN/C catalyst, because the coordination number of Ni−Ni (CN_{Ni-Ni}) derived by the EXAFS fitting is 3.5 ± 0.9 (see Table 3), although this number should be larger than 10 for a core with a 2.44 nm diameter consisting of only Ni atoms.[28]

Next, we assume that the shell comprises one-ML of Pt atoms, and the core forms a solid solution structure of PtNi (Pt 1ML-shell model in Figure 7b). The probability that Pt surface

https://doi.org/10.1021/acsaem.2c00631
ACS Appl. Energy Mater. 2022, 5, 5245−5255

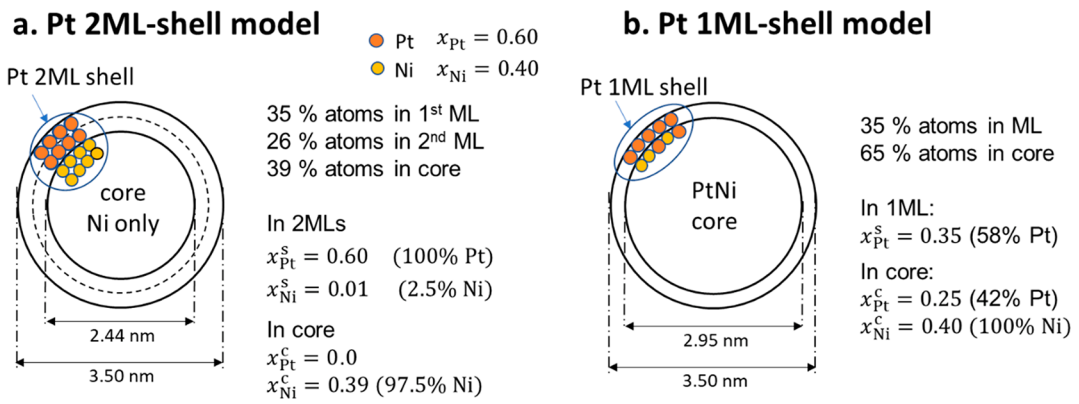

Figure 7. Schematics of (a) a Pt 2ML-shell model and (b) Pt 1ML-shell model for PtNi nanoparticles with a particle size of 3.5 nm and a Pt:Ni mole ratio of 0.6:0.4.

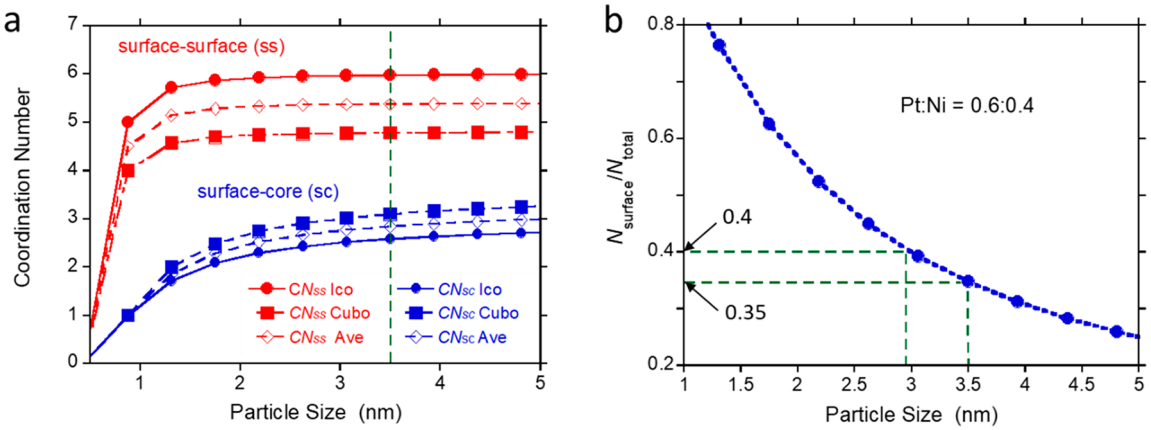

Figure 8. (a) Coordination numbers of surface−surface (ss) atoms (CN_{ss}) and surface−core (sc) atoms (CN_{sc}) for icosahedrons (Ico) and cuboctahedrons (Cubo), and (b) ratio of surface atoms ($N_{surface}$) to total atoms (N_{total}) calculated from a theoretical nanocluster model, plotted versus particle size.[30] The particle sizes were calculated from a volume-correlated sphere model[28] using an average diameter d = 0.262 nm (= 0.60 (Pt mole ratio) × 0.276 nm (Pt diameter) + 0.40 (Ni mole ratio) × 0.242 nm (Ni diameter)).

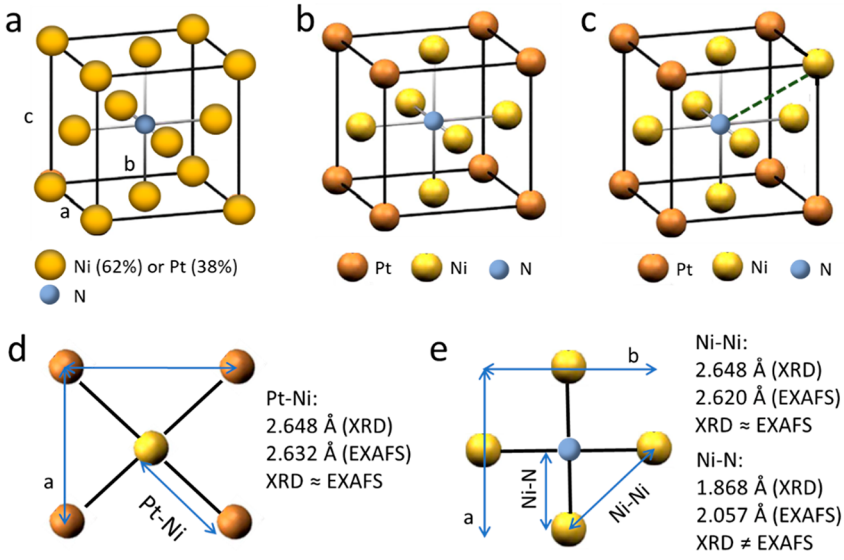

Figure 9. $(Pt_xNi_{1-x})_4N$ core models where (a) Ni (62%) and Pt (38%) atoms are sited randomly at the external fcc sites, (b) Ni atoms are preferentially located at the centers of fcc faces, while Pt atoms are sited at the corners, and (c) Ni atoms are sited at the face centers and a few corners of the fcc structure, while Pt atoms occupy the other corners. In all the models, a N atom occupies the cube center. Schematics of (d) an upper or lower plane of the (b) model with Pt−Ni distances, and (e) a middle plane of the (b) model with Ni−Ni and Ni−N distances from XRD and EXAFS.

https://doi.org/10.1021/acsaem.2c00631
ACS Appl. Energy Mater. 2022, 5, 5245−5255

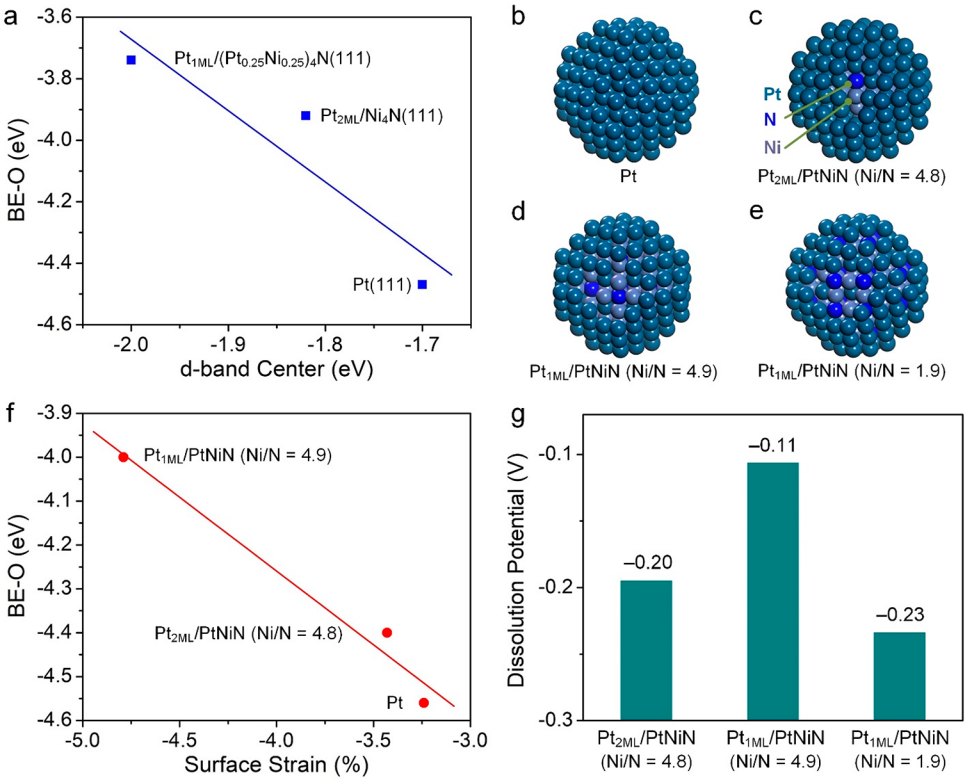

Figure 10. (a) Comparison of d-band center versus binding energy of oxygen (BE-O) on three extended surfaces of Pt(111), $Pt_{2ML}/Ni_4N(111)$, and $Pt_{1ML}/(Pt_{0.25}Ni_{0.75})_4N(111)$. Geometrical illustration of (b) a Pt nanoparticle, (c) 2ML core−shell Pt_{2ML}/PtNiN (Ni/N = 4.8), (d) 1ML core−shell Pt_{1ML}/PtNiN (Ni/N = 4.9), and (e) 1ML core−shell Pt_{1ML}/PtNiN (Ni/N = 1.9). The atom numbers for each model are described in Table S2. (f) Calculated surface strain versus BE-O on three sphere-like nanoparticle models of Pt, Pt_{2ML}/PtNiN (Ni/N = 4.8), and Pt_{1ML}/PtNiN (Ni/N = 4.9) with a particle size of ∼1.7 nm. (g) Calculated dissolution potentials of core−shell Pt_{2ML}/PtNiN (Ni/N = 4.8), Pt_{1ML}/PtNiN (Ni/N = 4.9), and Pt_{1ML}/PtNiN (Ni/N = 1.9) models.

atoms coordinate with Pt atoms in the core is given by the molar ratio of Pt in the PtNi core. As mentioned above, the single Pt ML shell uses 35% of the total atoms, N_{total} ($N_{surface}/N_{total}$ = 0.35 in Figure 8b), and thus, the core comprises all of the Ni (40% of N_{total} atoms) and the remaining Pt (25% of N_{total} atoms). Figure 8a shows CNs of surface−surface (ss) atoms (CN_{ss}) and surface−core (sc) atoms (CN_{sc}) for icosahedra (Ico) and cuboctahedra (Cubo), which are thought as likely structures of Pt-based nanoparticles,[29] calculated from a theoretical nanocluster model plotted versus particle size.[28,30−32] The CN_{ss} numbers for a 3.5 nm particle are 5.98 and 4.88 for Ico and Cubo, respectively, and the average is 5.43. Similarly, the N_{sc} numbers for a 3.5 nm particle are 2.60 and 3.07 for Ico and Cubo, respectively, and the average is 2.83. The probability of Pt surface atoms coordinating with Pt atoms in the core is given by the mole ratio of Pt in a PtNi core, which is calculated to be 0.38 (= 0.25/(0.25 + 0.4)). Using this model, the coordination number of surface Pt and core Pt atoms is 1.09 (= 2.83 × 0.38), and thus, a theoretical Pt−Pt coordination number is 6.51 (5.43 + 1.09), which is consistent with the EXAFS fitting result (6.4 ± 0.6).

The previous synchrotron XRD analysis demonstrated that the PtNiN/C synthesized by the two-step method has a structure comprising Ni_4N cores encapsulated by multilayer Pt shells (≥2 shells).[15] In the present system, the core must include Pt atoms, and thus, an fcc-$(Pt_xNi_{1-x})_4N$ core structure is considered. To develop a more detailed PtNiN core atomic model, we hypothesize a first model (a) where Pt and Ni atoms are sited randomly at external fcc sites with a N atom at a center of an fcc structure as illustrated in Figure 9a. Since 62% of the core atoms are Ni, ∼3.7 out of the 6 face positions will be occupied by Ni. It has been reported that the formation of noble metal nitrides including platinum nitrides requires extremely high pressures and high temperatures (for example, ∼50 GPa and 1727 °C for PtN).[33−35] For this reason, we consider a second atomic model (b) where Ni atoms are preferentially located at the centers of fcc faces and Pt atoms are at the corners (Figure 9b). We must also consider the XRD analysis, which indicates that the PtNiN/C catalyst is an fcc structure with a lattice constant of 3.736 Å. Figure 9d depicts an upper or lower fcc plane of the atomic model shown in Figure 9b. The Pt−Ni distance derived from the XRD analysis is 2.648 Å ($\sqrt{2}$ × 3.736 Å), which is in good agreement with the Pt−Ni distance derived from EXAFS fitting (2.632 Å). Figure 9d shows the middle plane of the fcc atomic model illustrated in Figure 9b; the Ni−Ni distance from the XRD analysis is 2.648 Å, which is also in good agreement with that determined from the EXAFS fitting (2.620 Å). However, the Ni−N distance estimated from the XRD is 1.864 Å (=3.736/2), which is much shorter than that from the EXAFS fitting (2.057 Å). Because the EXAFS is an elemental-specific measurement, we believe that the EXAFS fitting result for the Ni−N distance is more accurate than that estimated from XRD. Therefore, we hypothesize a third model (c) where Ni atoms also occupy a few corners of the fcc structure as depicted in Figure 9c. In the case that Ni−N distance is longer (3.240 Å), and if a Ni atom occupies one corner, the average Ni−N distance (2.040 Å) is close to that of EXAFS fitting

https://doi.org/10.1021/acsaem.2c00631
ACS Appl. Energy Mater. 2022, 5, 5245−5255

(2.057 Å). Thus, the third model (Figure 9c) represents the PtNiN core structure better than the other two models (Figure 9a,b). The EXAFS/XRD analysis, therefore, suggests that the one-step PtNiN/C catalyst comprises a Pt ML shell on the $(Pt_xNi_{1-x})_4N$-type core model, in which Ni atoms occupy the face centers and a few of the corners of an fcc structure, Pt atoms occupy the other corners of an fcc cube, and N occupies the cube center (Figure 9c).

DFT-Based Studies. To provide more insight into the PtNiN/C structure discussed above, we carried out DFT calculations. We first optimized a bulk model of Ni_4N ($a_{0,DFT}$ = 3.7622 Å) and $(Pt_{0.25}Ni_{0.75})_4N$ ($a_{0,DFT}$ = 3.8289 Å) used for a core material (Figure S5) to computationally support the experiment-based $(Pt_xNi_{1-x})_4N$ core model (Figure 9c). $(Pt_{0.25}Ni_{0.75})_4N$ exhibits a slight expansion of 1.8% compared to Ni_4N due to the Pt replacement ($a_{0,DFT}$ = 4.0026 Å). The calculated geometrical parameters of Ni_4N and $(Pt_{0.25}Ni_{0.75})_4N$ are reasonably in agreement with those from XRD and EXAFS experiments (Table S2). Before carrying out theoretical analyses using nanoparticle models, we first accounted for DFT-based descriptors of the d-band center and the binding energy of oxygen (BE-O) using the extended surfaces of Pt(111), $Pt_{2ML}/Ni_4N(111)$, and $Pt_{1ML}/(Pt_{0.25}Ni_{0.75})_4N(111)$, referring to Pt/C, two-step-synthesized PtNiN/C with two ML Pt shells on Ni_4N cores, and one-step-synthesized PtNiN/C with one ML Pt shell on $(Pt_{0.25}Ni_{0.75})_4N$ cores, respectively, as shown in Figure S5. As depicted in Figure 10a, the core−shell configurations with Ni and N result in a more downshifted Pt d-band center (−2.00 eV for $Pt_{1ML}/(Pt_{0.25}Ni_{0.75})_4N(111)$, −1.82 eV for $Pt_{2ML}/Ni_4N(111)$, and −1.70 eV for Pt(111)) and a weaker BE-O (−3.74 eV for $Pt_{1ML}/(Pt_{0.25}Ni_{0.75})_4N(111)$, −3.92 eV for $Pt_{2ML}/Ni_4N(111)$, and −4.47 eV for Pt(111)) compared to pure Pt(111). The extended surface model accurately explains how the BE-O correlates with the ORR activities, confirming ORR activities of one-step-synthesized PtNiN/C > two-step-synthesized PtNiN/C > Pt/C. The extended surface model may not accurately project the surface strain effect, since half of the bottom layers are fixed at the bulk parameters (Pt, Ni_4N, or $(Pt_{0.25}Ni_{0.75})_4N$). Thus, to investigate the descriptor's influence of surface strain, we performed more realistic calculations using ∼1.7 nm nanoparticle models as shown in Figure 10b−e. We first examined the effect of N concentration (Ni/N = 1.9, 4.8, and 4.9) using three core−shell models (Figure S6 and Table S3). It was geometrically confirmed that too much N addition causes irregular surfaces, resulting in instability of nanoparticles and an unreasonable binding energy of oxygen. Thus, to be aligned with the experimental Ni/N atomic ratio of 5.5, we applied the Pt_{1ML}/PtNiN (Ni/N = 4.9) model for further detailed calculations along with Pt_{2ML}/PtNiN (Ni/N = 4.8). Figure 10f shows the surface strain versus BE-O for the nanoparticle models, in which the nitrided core modifies the surface contraction, making a more strained surface, shifting from −3.24% (Pt) to −3.43% (Pt_{2ML}/PtNiN, Ni/N = 4.8) and −4.79% (Pt_{1ML}/PtNiN, Ni/N = 4.9). The more compressive strain of Pt_{1ML}/PtNiN than Pt_{2ML}/PtNiN may also support the ORR enhancement of one-step-synthesized PtNiN/C compared to two-step-synthesized PtNiN/C. To explain the excellent stability of the one-step PtNiN/C, we also assume that during the formation of nitride core−shell materials, diffusion of Pt atoms to vacancies at the vertex of the shell occurs to fill the vacancy sites due to the segregation effect of noble metals.[15] To further confirm the relative stability, we conducted dissolution potential calculations of the three core−shell nanoparticle models (Figure 10g). As the N concentration increases from Ni/N = 4.9 to 1.9, the dissolution potential decreases from −0.11 to −0.23 V, indicating that reducing the Pt concentration in the core from Pt_{2ML}/PtNiN (60 Pt atoms) to Pt_{1ML}/PtNiN (20 Pt atoms) (Table S3) lowers the dissolution potential. This calculation indicates that the Pt_{1ML}/PtNiN model (Ni/N = 4.9) is more stable than Pt_{2ML}/PtNiN (Ni/N = 4.8) and Pt_{1ML}/PtNiN (Ni/N = 1.9). Overall, our DFT-based investigation confirms the experimental finding of the higher ORR activities of N-doped Pt-metal electrocatalysts with the 1ML core−shell configuration than the 2ML core−shell structure. It elucidates that the interactions of Pt/C and two-step-synthesized PtNiN/C with oxygen are too strong compared to one-step-synthesized PtNiN/C. The new synthesis approach improves the ORR activity and stability because of both geometric and electronic effects.

CONCLUSIONS

We have developed a one-step method to synthesize a highly active and durable N-doped PtNiN/C ORR catalyst for use in PEMFCs. The one-step PtNiN/C catalyst showed enhanced ORR activity in RDE testing, which is higher than that synthesized by the previous two-step synthesis. The MA loss after the 30 000 cycles of ADT testing was only 30%. MEA fuel cell testing of this catalyst demonstrated improved BOL activity and superb durability, with only 19 and 13% losses in MA and ECSA after 30 000 ADT cycles, respectively. *In situ* XAS coupled with the XRD analyses confirmed the formation of Pt ML shells on $(Pt_xNi_{1-x})_4N$-structured cores, where N is located at the center of an fcc structure. The origins of the enhanced activity and stability of the PtNiN/C catalyst synthesized by the one-step method are elucidated by DFT calculations combined with the experimental results. The present study demonstrates that the highly active and durable ORR catalyst can be produced by a simple one-step method, which is suitable for large-scale synthesis for producing greater than 1 g of catalyst. The establishment of this one-step synthesis method is expected to accelerate the transition of the N-doped PtNiN catalyst toward commercial viability, particularly for heavy-duty truck applications where high catalytic durability is required. Further electrode design and MEA process optimization are required to improve performance and stability at high-current-density regions.

ASSOCIATED CONTENT

Supporting Information

The Supporting Information is available free of charge at https://pubs.acs.org/doi/10.1021/acsaem.2c00631.

TEM-EDS analysis, fcc structure models, CV curves and ECSA in MEA testing, voltage losses in MEA testing, procedures of DFT calculations, table of MEA performance in literature, table of experimental and theoretical bond distances, and table of the number of atoms used for the DFT models (PDF)

AUTHOR INFORMATION

Corresponding Author

Kotaro Sasaki − *Chemistry Division, Brookhaven National Laboratory, Upton, New York 11973, United States;*

https://doi.org/10.1021/acsaem.2c00631
ACS Appl. Energy Mater. 2022, 5, 5245−5255

orcid.org/0000-0003-2474-8323; Email: ksasaki@bnl.gov

Authors

Liang Song − *Chemistry Division, Brookhaven National Laboratory, Upton, New York 11973, United States; Department of Materials Science and Chemical Engineering, Stony Brook University, Stony Brook, New York 11790, United States*

Yun Cai − *Global Fuel Cell Business, General Motors, Pontiac, Michigan 48340, United States;* Present Address: General Motors R&D Center, Warren, Michigan 48092, United States

Yang Liu − *Department of Materials Science and Chemical Engineering, Stony Brook University, Stony Brook, New York 11790, United States;* orcid.org/0000-0003-4347-1729

Xueru Zhao − *Chemistry Division, Brookhaven National Laboratory, Upton, New York 11973, United States*

Kurian A. Kuttiyiel − *Chemistry Division, Brookhaven National Laboratory, Upton, New York 11973, United States*

Nebojsa Marinkovic − *Synchrotron Catalysis Consortium and Department of Chemical Engineering, Columbia University, New York, New York 10027, United States*

Anatoly I. Frenkel − *Chemistry Division, Brookhaven National Laboratory, Upton, New York 11973, United States; Department of Materials Science and Chemical Engineering, Stony Brook University, Stony Brook, New York 11790, United States;* orcid.org/0000-0002-5451-1207

Anusorn Kongkanand − *Global Fuel Cell Business, General Motors, Pontiac, Michigan 48340, United States*

YongMan Choi − *College of Photonics, National Yang Ming Chiao Tung University, Tainan 71150, Taiwan*

Radoslav R. Adzic − *Chemistry Division, Brookhaven National Laboratory, Upton, New York 11973, United States*

Complete contact information is available at: https://pubs.acs.org/10.1021/acsaem.2c00631

Notes

The authors declare no competing financial interest.

■ ACKNOWLEDGMENTS

This manuscript has been authored by employees/guests of Brookhaven Science Associates, LLC, under Contract No. DE-SC0012704 with the U.S. Department of Energy (DOE). The publisher by accepting the manuscript for publication acknowledges that the United States Government retains a nonexclusive, paid-up, irrevocable, worldwide license to publish or reproduce the published form of this manuscript, or allow others to do so, for United States Government purposes. Additional work was performed by the Million Mile Fuel Cell Truck (M2FCT) Consortium (https://millionmilefuelcelltruck.org), technology manager Greg Kleen, which is supported by the U.S. DOE, Office of Energy Efficiency and Renewable Energy, Hydrogen and Fuel Cell Technologies Office, under Contract No. DE-SC0012704 (Brookhaven National Laboratory). The EXAFS analysis by Y.L. and A.I.F. was supported as part of the Integrated Mesoscale Architectures for Sustainable Catalysis (IMASC), an Energy Frontier Research Center funded by the U.S. Department of Energy, Office of Science, Basic Energy Sciences under Award DE-SC0012573. This work is also performed in collaboration with General Motors under Contract No. NF-17-33. This research used the resources of the Center for Functional Nanomaterials and the QAS (7-BM) and ISS (8-ID) beamlines of the National Synchrotron Light Source II, which are U.S. DOE Office of Science Facilities, at Brookhaven National Laboratory under Contract No. DE-SC0012704. Additional resources at the QAS beamline were provided by the Synchrotron Catalysis Consortium, which is supported by the U.S. DOE, Office of Basic Energy Sciences, under Grant No. DE-SC0012335. Computational studies were supported by the Ministry of Science and Technology (MOST Grant No. 110-2221-E-A49-017-MY3), the National Center for High-performance Computing (NCHC), and the Higher Education Sprout Project of the National Yang Ming Chiao Tung University and Ministry of Education (MOE), Taiwan.

■ REFERENCES

(1) Debe, M. K. Electrocatalyst approaches and challenges for automotive fuel cells. *Nature* **2012**, *486*, 43−51.

(2) Shao, M. H.; Chang, Q. W.; Dodelet, J. P.; Chenitz, R. Recent advances in electrocatalysts for oxygen reduction reaction. *Chem. Rev.* **2016**, *116*, 3594−3657.

(3) Stamenkovic, V. R.; Strmcnik, D.; Lopes, P. P.; Markovic, N. M. Energy and fuels from electrochemical interfaces. *Nat. Mater.* **2017**, *16*, 57−69.

(4) Sasaki, K.; Shao, M.; Adzic, R. R. Dissolution and stabilization of platinum in oxygen cathodes. *Polymer Electrolyte Fuel Cell Durability* **2009**, 7−27.

(5) Sasaki, K.; Naohara, H.; Cai, Y.; Choi, Y. M.; Liu, P.; Vukmirovic, M. B.; Wang, J. X.; Adzic, R. R. Core-protected core-shell electrocatalysts − potential for automotive applications of fuel cells. *Angew. Chem., Int. Ed.* **2010**, *49*, 8602−8607.

(6) Sasaki, K.; Naohara, H.; Choi, Y. M.; Cai, Y.; Chen, W.-H.; Liu, P.; Adzic, R. R. Highly stable Pt monolayer on PdAu nanoparticle electrocatalysts for the oxygen reduction reaction. *Nat. Commun.* **2012**, *3*, 1115.

(7) Sasaki, K.; Wang, J. X.; Naohara, H.; Marinkovic, N.; More, K.; Inada, H.; Adzic, R. R. Recent advances in platinum monolayer electrocatalysts for oxygen reduction reaction: Scale-up synthesis, structure and activity of Pt shells on Pd cores. *Electrochim. Acta* **2010**, *55*, 2645−2652.

(8) Adzic, R. R.; Marinkovic, N. *Platinum Monolayer Electrocatalysts*; Springer, 2020.

(9) Sasaki, K.; Kuttiyiel, K. A.; Adzic, R. R. Designing high performance Pt monolayer core−shell electrocatalysts for fuel cells. *Curr. Opin. Electrochem.* **2020**, *21*, 368−375.

(10) Wang, C.; Chi, M. F.; Li, D. G.; Strmcnik, D.; van der Vliet, D.; Wang, G. F.; Komanicky, V.; Chang, K. C.; Paulikas, A. P.; Tripkovic, D.; Pearson, J.; More, K. L.; Markovic, N. M.; Stamenkovic, V. R. Design and synthesis of bimetallic electrocatalyst with multilayered Pt-Skin surfaces. *J. Am. Chem. Soc.* **2011**, *133* (36), 14396−14403.

(11) Toda, T.; Igarashi, H.; Uchida, H.; Watanabe, M. Enhancement of the electroreduction of oxygen on Pt alloys with Fe, Ni, and Co. *J. Electrochem. Soc.* **1999**, *146* (10), 3750−3756.

(12) Debe, M. K.; Steinbach, A. J.; Vernstrom, G. D.; Hendricks, S. M.; Kurkowski, M. J.; Atanasoski, R. T.; Kadera, P.; Stevens, D. A.; Sanderson, R. J.; Marvel, E.; Dahn, J. R. Extraordinary oxygen reduction activity of Pt_3Ni_7. *J. Electrochem. Soc.* **2011**, *158*, B910−B918.

(13) Rao, C. V.; Viswanathan, B. ORR activity and direct ethanol fuel cell performance of carbon-supported Pt−M (M = Fe, Co, and Cr) alloys prepared by polyol reduction method. *J. Phys. Chem. C* **2009**, *113*, 18907−18913.

(14) Kuttiyiel, K. A.; Choi, Y.; Hwang, S.-M.; Park, G.-G.; Yang, T.-H.; Su, D.; Sasaki, K.; Liu, P.; Adzic, R. R. Enhancement of the oxygen reduction on nitride stabilized Pt-M (M = Fe, Co, and Ni) core−shell nanoparticle electrocatalysts. *Nano Energy* **2015**, *13*, 442−449.

(15) Kuttiyiel, K. A.; Sasaki, K.; Choi, Y. M.; Su, D.; Liu, P.; Adzic, R. R. Nitride stabilized PtNi core-shell nanocatalyst for high oxygen reduction activity. *Nano Lett.* **2012**, *12* (12), 6266−6271.
(16) Zhou, M.; Wang, H.; Elnabawy, A. O.; Hood, Z. D.; Chi, M.; Xiao, P.; Zhang, Y.; Mavrikakis, M.; Xia, Y. Facile one-pot synthesis of Pd@Pt_{1L} octahedra with enhanced activity and durability toward oxygen reduction. *Chem. Mater.* **2019**, *31*, 1370−1380.
(17) Gasteiger, H. A.; Kocha, S. S.; Sompalli, B.; Wagner, F. T. Activity benchmarks and requirements for Pt, Pt-alloy, and non-Pt oxygen reduction catalysts for PEMFCs. *Appl. Catal., B* **2005**, *56*, 9−35.
(18) Sasaki, K.; Marinkovic, N.; Isaacs, H. S.; Adzic, R. R. Synchrotron-based in situ characterization of carbon-supported platinum and platinum monolayer electrocatalysts. *ACS Catal.* **2016**, *6*, 69−76.
(19) Ravel, B.; Newville, M. ATHENA, ARTEMIS, HEPHAESTUS: data analysis for X-ray absorption spectroscopy using IFEFFIT. *Synchrotron Radiat.* **2005**, *12*, 537−541.
(20) Kresse, G.; Furthmuller, J. Efficient iterative schemes for ab initio total-energy calculations using a plane-wave basis set. *Phys. Rev. B* **1996**, *54*, 11169−11186.
(21) Perdew, J. P.; Burke, K.; Ernzerhof, M. Generalized gradient approximation made simple. *Phys. Rev. Lett.* **1996**, *77* (18), 3865−3868.
(22) Greeley, J.; Nørskov, J. K. Electrochemical dissolution of surface alloys in acids: Thermodynamic trends from first-principles calculations. *Electrochim. Acta* **2007**, *52*, 5829−5836.
(23) Garsany, Y.; Baturina, O. A.; Swider-Lyons, K. E.; Kocha, S. S. Experimental methods for quantifying the activity of platinum electrocatalysts for the oxygen reduction reaction. *Anal. Chem.* **2010**, *82*, 6321−6328.
(24) Zhao, X.; Xi, C.; Zhang, R.; Song, L.; Wang, C.; Spendelow, J. S.; Frenkel, A. I.; Yang, J.; Xin, H. L.; Sasaki, K. High-performance nitrogen-doped intermetallic PtNi catalyst for the oxygen reduction reaction. *ACS Catal.* **2020**, *10*, 10637−10645.
(25) Kongkanand, A.; Mathias, M. F. The priority and challenge of high-power performance of low platinum proton-exchange membrane fuel cells. *J. Phys. Chem. Lett.* **2016**, *7*, 1127−1137.
(26) Lytle, F. W.; Wei, P. S. P.; Greegor, R. B.; Via, G. H.; Sinfelt, J. H. Effect of chemical environment on magnitude of x-ray absorption resonance at L_{III} edges. Studies on metallic elements, compounds, and catalysts. *J. Chem. Phys.* **1979**, *70*, 4849−4855.
(27) Horsley, J. A. Relationship between the area of $L_{2,3}$ x-ray absorption edge resonances and the *d* orbital occupancy in compounds of platinum and iridium. *J. Chem. Phys.* **1982**, *76*, 1451−1458.
(28) Marinkovic, N. S.; Sasaki, K.; Adzic, R. R. Determination of single- and multi-component nanoparticle sizes by X-ray absorption spectroscopy. *J. Electrochem. Soc.* **2018**, *165*, J3222−J3230.
(29) McBreen, J.; Mukerjee, S. *In situ* x-ray absorption studies of carbon-supported Pt and Pt alloy nanoparticles. In *Interfacial Electrochemistry: Theory, Experiment, and Applications*; Wieckowski, A., Ed.; Marcel Dekker: New York, 1999; pp 895−913.
(30) Montejano-Carrizales, J. M.; Aguilera-Granja, F.; Moran-Lopez, J. L. Direct enumeration of the geometrical characteristics of clusters. *NanoStruct. Mater.* **1997**, *8* (3), 269−287.
(31) Glasner, D.; Frenkel, A. I. Geometrical characteristics of regular polyhedra: Application to EXAFS studies of nanoclusters. *AIP Conf. Proc.* **2006**, *2007*, 746−748.
(32) Frenkel, A. I.; Yevick, A.; Cooper, C.; Vasic, R. Modeling the structure and composition of nanoparticles by EXAFS. *Annu. Rev. Anal. Chem.* **2011**, *4*, 23−39.
(33) Crowhurst, J. C.; Goncharov, A. F.; Sadigh, B.; Evans, C. L.; Morrall, P. G.; Ferreira, J. L.; Nelson, A. J. Synthesis and characterization of the nitrides of platinum and iridium. *Science* **2006**, *311*, 1275−1278.
(34) Gregoryanz, E.; Sanloup, C.; Somayazulu, M.; Badro, J.; Fiquet, G.; Mao, H. K.; Hemley, R. J. Synthesis and characterization of a binary noble metal nitride. *Nat. Mater.* **2004**, *3*, 294−297.
(35) von Appen, J.; Lumey, M. W.; Dronskowski, R. Mysterious platinum nitride. *Angew. Chem., Int. Ed.* **2006**, *45*, 4365−4368.

https://doi.org/10.1021/acsaem.2c00631
ACS Appl. Energy Mater. 2022, 5, 5245−5255